On Construction of Trajectory of Boxer's Punch using a single IMU

Yu-Cheng Lee[1], Kai-Po Hsu[1], Yun-Ju Lee[1], Yi-Ting Li[1], Yung-Chih Chen[2], Wen-Hsin Chiu[1], and Chun-Yao Wang[1]

[1]National Tsing Hua University, Taiwan, ROC
[2]National Taiwan University of Science and Technology, Taiwan, R.O.C.

***Abstract*—In this work, we propose a system to construct the trajectory of punch for boxers. This system can plot trajectories of three kinds of punches including straight punch, hook, and uppercut via a single IMU sensor. A quaternion-based approach is utilized to identify rotations on collected data in three-dimensional space. Furthermore, we apply ellipsoid fitting as our calibration method to remove the built-in offsets inside the IMU sensor effectively. The experimental results show that the proposed system achieves reliable trajectories compared to the professional motion capture product, VICON Motion Systems. The root mean square error ($RMSE$) of trajectory in straight punch, hook, and uppercut are 0.041m, 0.078m, and 0.117m, respectively.**

I. Introduction

In recent years, sport performance monitoring is becoming increasingly important for athletes. One of the focuses in sport performance monitoring is motion analysis. Correct and smooth movements lead athletes to achieve better results. Traditionally, a camera-based motion analysis system, such as VICON Motion Systems [20], is utilized to capture trajectories for different kinds of sports, which allows athletes to recognize their motions instantaneously. Furthermore, when coaches want to adjust the posture of players, they have evidence based on the real-time trajectories.

With such precise motion capture systems, we obtain accurate 3D trajectory of any movements. However these systems have some drawbacks. First, they suffer from environmental restrictions, such as a spacious room, and setup angles of multiple cameras. Second, they require pre-calibration and post-processing, which is time-consuming, to obtain the final trajectory result. Last, they are quite expensive. These drawbacks restrict the motion capture systems to be popular in sports.

An inertial measurement unit (IMU) is usually composed of an accelerometer, a gyroscope, and a magnetometer. People mostly use these portable devices for gait analysis [4] [11] [12] [17], activity classification [6] [10] [14] [15] [17] [18] [19], rehabilitation monitoring [2] [7], etc. Moreover, due to IMU sensors' compact size and low cost, they have gained widespread usage in sport performance monitoring. Among them, 3D trajectory construction is a significant component in sport performance monitoring. In fact, there have been some works about the construction of trajectory with the aid of IMU sensors [1] [3] [5] [9] [16]. In [5], the authors introduced a deep learning model to estimate the lower limbs' trajectory while the person is walking. In [9], an algorithm was developed to construct the handwriting trajectory using a single IMU sensor. In [3], a study was proposed to obtain a trajectory of people walking in indoor environment by a deep neural network framework.

By reading the trajectories of the movements, athletes can have a better understanding of the fluency of their movements. Additionally, it is easier for coaches to give guidance on movements and modify the details of movements when necessary. Hence, there are some studies about the 3D trajectory construction of different sports, which are more related to our work. In [1] and [16], the authors proposed to calculate the swing trajectory in golf and kicking trajectory in soccer with the data collected from IMU sensors. Both of these studies [1] [16] utilized quaternion techniques to calculate rotations in the space.

Compared to the aforementioned sports of golf [1] and soccer [16], boxing is a relatively fast-paced sport. Every sequence of punches happens in a short period of time at high speed. As a result, unlike the two studies mentioned above, when plotting the trajectories of punches, we need to first segment the collected data. Once the data is segmented into individual punch, we can then proceed with the construction of trajectories. On the contrary, the reason why [1] [16] do not require data segmentation is that they do not involve continuous high-speed movements. Therefore, they can directly plot the trajectories without cumulative errors. Another difference in plotting trajectories of punches is that the range of motion is relatively small such that we cannot tolerate significant errors. To address this issue, we propose to employ different calibration methods on the accelerometer and gyroscope to remove the IMU sensor's offsets and noises effectively.

In this paper, we take boxing as the target sport, and propose a motion-tracking algorithm using accelerometer and gyroscope data. Our goal is to construct a precise trajectory while throwing punches. We aim to achieve similar results as a professional motion camera system, VICON Motion Systems [20], using just one IMU sensor.

The remainder of the paper is structured as follows. We introduce the IMU sensor we used and the background of quaternion in Section II. In Section III, we present the proposed approach. In Section IV, the experimental results are presented. Finally, we conclude this work in Section V.

II. Preliminaries

A. IMU Sensor

We develop a motion-tracking system with an IMU sensor designed and developed by Sea Land Technology, Inc [21]. The IMU sensor is comprised of several components, including a tri-axis accelerometer, a tri-axis gyroscope, a tri-axis magnetometer, a 3.3V lithium-ion battery, a wireless USB receiver, and a Micro USB connector for charging. The sensor is with dimensions of 20mm x 38mm x 8.5mm and weighs approximately 5g. The sampling rate is 400 Hz, which means 400 data will be received in 1 second. Additionally, the IMU sensor will be attached to one wrist of boxer for collecting data.

B. Quaternion

Euler angle and quaternion are two frequently used methods for calculating rotation in 3D space. Euler angle describes a rotation by multiplying three rotation matrices together. These rotation matrices are derived from the rotation angles around the X, Y, and Z axis, respectively. However, it is important to note that the order of multiplying these rotation

matrices is crucial, and different orders will result in different rotation effects. Although the Euler angle is easy to use, it would encounter a problem called singularity, which loses one dimension of rotation under a certain angle. In that case, we cannot express the rotation we have achieved. Thus, in this work, we use quaternion instead to express the rotation in 3D space.

Quaternion q is a vector that contains one real number a and three imaginary numbers bi, cj, dk, as shown in EQ(1),

$$q = a + bi + cj + dk \tag{1}$$

where $i^2 = j^2 = k^2 = ijk = -1$. The aforementioned relationship is established in quaternion world. This is because when an i, j, or k is multiplied, it represents a rotation in a 4D space. This relationship cannot be viewed directly with the ordinary definition of imaginary number. Moreover, the quaternion possesses its distinctive rules of multiplication, e.g., the multiplication of the quaternion's imaginary units is non-commutative, as expressed in EQ(2).

$$\begin{cases} ij = k,\ ji = -k \\ jk = i,\ kj = -i \\ ki = j,\ ik = -j \end{cases} \tag{2}$$

Additionally, a quaternion q can be represented as EQ(3),

$$q = cos(\frac{\theta}{2}) + sin(\frac{\theta}{2})u \tag{3}$$

where it rotates θ° around the rotation axis, u-axis. We only need one quaternion to achieve a rotation in 3D space. Moreover, when it comes to rotating the coordinate $p = (p_x, p_y, p_z)$ in 3D space by θ° with the quaternion q, we can achieve the rotation by using EQ(4),

$$p^{'} = qp\bar{q} \tag{4}$$

where $p^{'} = (p_x^{'}, p_y^{'}, p_z^{'})$ represents the new coordinate after the rotation, and $\bar{q}$ is the conjugate of q.

III. Proposed Approach

In this section, we present our approach. We explain the methods of collecting data, calibrating the IMU sensor, and plotting the trajectories of punches. The considered punches includes straight punch, hook, and uppercut.

A. Data Segmentation

This subsection discusses how we segment a sequence of punches. When a boxer executes a sequence of punches, each punch will be segmented with the corresponding trajectory. We use several criteria to determine whether a boxer is moving or not. Then, the data representing movement will be utilized to plot the corresponding trajectory.

Here are several parameters that are used in this work. First, we set a baseline threshold $threshold_x$ for X-axis, defined as EQ(5).

$$threshold_x = \frac{1}{400}\sum_{j=1}^{400}\alpha_x^{steady}(j) \tag{5}$$

This parameter is used to determine whether the boxer is in motion or not. To find this threshold, we place the IMU sensor in a stationary state for one second, and average the collected data. We take the data of the X-axis as an example in EQ(5). However, in fact, the acceleration data of the Y-axis and Z-axis can be used as well. In that case, the threshold is set as $threshold_y$ and $threshold_z$, respectively. Next, the initial difference $diff_1$ refers to the difference between the first data point $a_x(1)$ in a segment and the $threshold_x$. Then, $diff_i$ represents the difference between the i^{th} data point $a_x(i)$ in a segment and the $threshold_x$.

$$diff_1 = \alpha_x(1) - threshold_x \tag{6}$$

$$diff_i = \alpha_x(i) - threshold_x \tag{7}$$

Last, we have Max, Min, and n, which refers to the maximum, minimum value, and the number of data, in the current segment, respectively.

$$Max = max\{\alpha_x(i)|i = 1, ..., n\} \tag{8}$$

$$Min = min\{\alpha_x(i)|i = 1, ..., n\} \tag{9}$$

With these defined parameters, we have three criteria to determine whether the boxer's hand is moving or not. According to the preliminary experiments, the first criterion is set as that the difference between $diff_i$ and $diff_1$ is smaller than or equal to $0.15g$ ($1g$ is defined by 9.81 m/s^2) as shown in EQ(10).

$$|diff_i - diff_1| <= 0.15 \tag{10}$$

The remaining two criteria are shown in EQ(11) and EQ(12). We examine the differences between the i^{th} data point and the maximum or minimum value within the current segment.

$$|\alpha_x(i) - Max| <= 0.1 \tag{11}$$

$$|\alpha_x(i) - Min| <= 0.1 \tag{12}$$

When the above three criteria are met simultaneously for 60 times consecutively, the boxer is considered as not moving; otherwise, he/she is moving. An example of data segmentation is illustrated in Fig. 1. It segments a sequence of punchings into four punches based on the criteria mentioned above. The gray dashed lines indicate that the boxer is moving. On the contrary, the black solid lines are determined as not moving.

B. Sensor Calibration

Every IMU sensor has built-in offsets due to different processes of manufacturing. Hence, we need to calibrate the IMU sensor after the data segmentation. The way to calibrate a gyroscope is as follows: Each axis should read 0° when the IMU sensor is not moving. However, we do not get such ideal data because of built-in offset. This offset is obtained by using EQ(13), i.e., we collect gyroscope data in a stationary state for 10 seconds (400 data points) and average them as the $gyro\_offset$ of each axis i.

$$gyro\_offset_i = \frac{1}{4000}\sum_{j=1}^{4000}\omega_i^{steady}(j) \tag{13}$$

After having the offset in each axis i, we remove the offset from the gyroscope raw data ω_i^{raw} for obtaining the calibrated gyroscope data ω_i^{cal}, as shown in EQ(14).

$$\omega_i^{cal} = \omega_i^{raw} - gyro\_offset_i \tag{14}$$

Next, when it comes to the accelerometers, our calibration method is different from the above. We applied Ellipsoid Fitting [8] as a calibration method for the accelerometer. According to Ellipsoid Fitting, the summation of the squares of X, Y, and Z axis acceleration data should be equal to one under a static state, expressed as EQ(15),

$$(\frac{x - x_0}{R_x})^2 + (\frac{y - y_0}{R_y})^2 + (\frac{z - z_0}{R_z})^2 = 1 \tag{15}$$

where x_0, y_0, and z_0 represent the center point of the ellipsoid and can be interpreted as offset. Furthermore, R_x, R_y, and R_z represent the radii of the ellipsoid's three axes and can be viewed as scaling factors. EQ(15) means that acceleration data

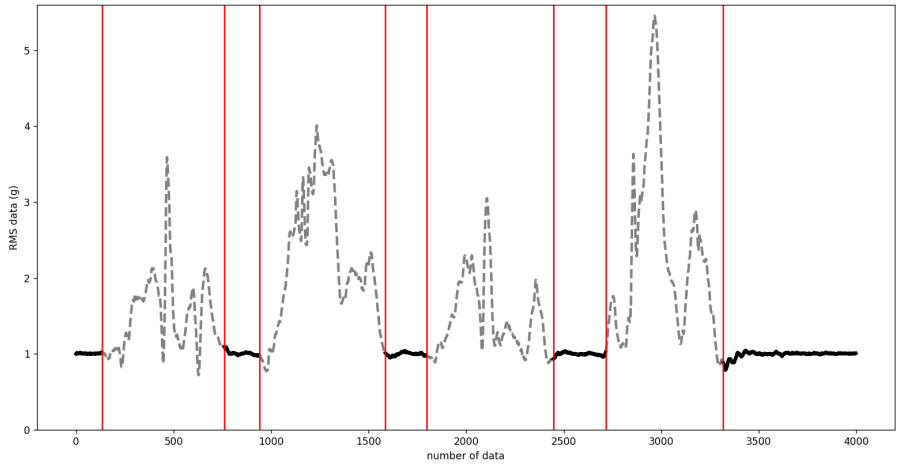

Fig. 1: The demonstration of data segmentation. The x-axis represents the data points collected during the period, and the y-axis represents the value of collected data.

collected at different stationary positions will be projected on an ellipse surface and form an ellipse sphere with a radius of one. Since we know that offsets O_i and scaling factors S_i exist in each sensor, the calibration problem can be expressed as EQ(16),

$$\begin{bmatrix} X_{true} \\ Y_{true} \\ Z_{true} \end{bmatrix} = \begin{bmatrix} S_0 & S_1 & S_2 \\ S_3 & S_4 & S_5 \\ S_6 & S_7 & S_8 \end{bmatrix} \begin{bmatrix} X_{raw} \\ Y_{raw} \\ Z_{raw} \end{bmatrix} + \begin{bmatrix} O_0 \\ O_1 \\ O_2 \end{bmatrix} \tag{16}$$

where X_{true}, Y_{true}, Z_{true} represent the true acceleration value and X_{raw}, Y_{raw}, Z_{raw} represent the raw data readings collected by the IMU sensor.

Next, we have to find out these calibration parameters, i.e., scaling factors $S_0 \sim S_8$, and offsets $O_0 \sim O_2$. EQ(16) can be written as EQ(17) by changing the order of the matrix multiplication.

$$\begin{bmatrix} X_{true} & Y_{true} & Z_{true} \end{bmatrix} = \begin{bmatrix} X_{raw} & Y_{raw} & Z_{raw} & 1 \end{bmatrix} \begin{bmatrix} S_0 & S_3 & S_6 \\ S_1 & S_4 & S_7 \\ S_2 & S_5 & S_8 \\ O_0 & O_1 & O_2 \end{bmatrix} \tag{17}$$

It will be more convenient to solve all these calibration parameters when they are in one matrix. Currently, this problem can be reformulated as EQ(18),

$$R = a \cdot K \tag{18}$$

where R is the matrix of true acceleration value, a is the matrix of raw data collected by the sensor at its six different stationary positions, and K is the matrix of 12 calibration parameters that need to be determined.

We sequentially rotate the IMU sensor to six known stationary positions, as shown in Fig. 2.

At each position, a_i will be collected from the IMU sensor, expressed as EQ(19),

$$a_i = [a_{xi}\ a_{yi}\ a_{zi}\ 1],\ i = 1 \sim 6 \tag{19}$$

where a_i is a 1x4 vector that represents the output readings of the accelerometer in one position. At the same time, R_i, which is a 1x3 vector, will be recorded as the true acceleration value at a specific position. For example, if the sensor is placed as Fig. 2(a), R will be recorded as EQ(20) due to the collection of $1g$ of gravity along the Z-axis in that specific position.

$$R = [0\ 0\ 1] \tag{20}$$

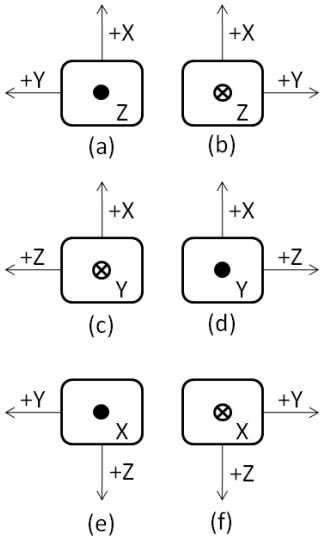

Fig. 2: The IMU sensor's three-axis defined directions at six different positions. The solid dot represents the positive direction of axis is facing outward. Conversely, the crossed dot indicates the positive direction of axis is facing inward.

After flipping the IMU sensor to all six positions, we combine all six a_i and R_i and have EQ(21).

$$R_{6\times3} = a_{6\times4} \cdot K_{4\times3} \tag{21}$$

Now, the desired calibration parameter matrix K can be determined by EQ(22).

$$\begin{aligned} a^T \cdot R &= (a^T \cdot a) \cdot K \\ (a^T \cdot a)^{-1} \cdot a^T \cdot R &= K \end{aligned} \tag{22}$$

In the later experiments, we have to apply the calibration on the raw acceleration data a^{raw} using the matrix K. Then, we can get the calibrated acceleration data a^{cal} like EQ(17). The equation is shown as EQ(23).

$$\begin{bmatrix} a_x^{cal} & a_y^{cal} & a_z^{cal} \end{bmatrix} = \begin{bmatrix} a_x^{raw} & a_y^{raw} & a_z^{raw} & 1 \end{bmatrix} \cdot K \tag{23}$$

C. Verification on Calibration

After calibrating the IMU, we carry out another verification step to ensure that the calibration is effective. We verify the calibration of the gyroscope by integrating angular velocity data under a known rotation angle. For example, we rotated the IMU sensor for $180°$ on the X-axis. Then, we will integrate uncalibrated and calibrated angular velocity on X-axis from the gyroscope to obtain the rotation angles. According to the comparison from the experimental results, our calibration improves the preciseness, which will be shown in the experimental results.

For the verification of calibrated accelerometer data, we use the similar method mentioned above. We integrate the uncalibrated and calibrated accelerometer values twice under a known distance. For example, we slid the IMU sensor toward +Y direction for 0.5m. Experimental result section will show the effectiveness of this calibration as well.

D. Orientation Adjustment

In general, to obtain the trajectory of a moving object, we just integrate the acceleration data collected from IMU sensor twice to get the object's displacement, and then combine these displacements at every time point. However, the punching trajectory cannot be calculated in this way. This is because the punching trajectory will be affected by both linear acceleration and angular acceleration in the raw data. If we directly integrate the collected acceleration data twice, the constructed trajectory might contain a significant error. In fact, the coordinate system of the IMU sensor will change as time goes on during the punching process. The collected data will not be in the same coordinate system such that the acceleration data cannot be integrated directly. Therefore, we have to rotate the acceleration data to the same reference coordinate system first. As mentioned in Section II.B, we use quaternion to consider rotation in 3D space.

We update the quaternion at every time point as shown in EQ(24),

$$q_t = q_{t-1} + \dot{q} \tag{24}$$

where quaternion at time t will be equal to quaternion at time t-1 plus the delta of quaternion over this period of time. The delta of the quaternion $\dot{q}$ can be written as EQ(25).

$$\dot{q} = \frac{1}{2} \begin{bmatrix} 0 & -\omega_x^{cal} & -\omega_y^{cal} & -\omega_z^{cal} \\ \omega_x^{cal} & 0 & -\omega_z^{cal} & -\omega_y^{cal} \\ \omega_y^{cal} & -\omega_z^{cal} & 0 & \omega_x^{cal} \\ \omega_z^{cal} & \omega_y^{cal} & -\omega_x^{cal} & 0 \end{bmatrix} \cdot q_{t-1} \tag{25}$$

In EQ(25), we utilize the calibrated gyroscope data ω_i^{cal} to compute the delta of the quaternion. After gaining quaternion q at every time point, we can perform a rotation on calibrated acceleration data a_i^{cal} to obtain the acceleration data after rotation a_i^{rot}. The purpose of the rotation is to make all calibrated acceleration data a_i^{cal} into the same coordinate system. EQ(26) describes how we rotate it,

$$a_i^{rot} = q \cdot a_i^{cal} \cdot \bar{q} \tag{26}$$

where a_i^{cal} is the calibrated acceleration data mentioned in Section III.B and can be viewed as the original coordinate; q is the quaternion at this moment, and $\bar{q}$ denotes the conjugate of q. Last, a_i^{rot} represents the new coordinate after the rotation. At this moment, we can confirm that all acceleration data are in the same coordinate system.

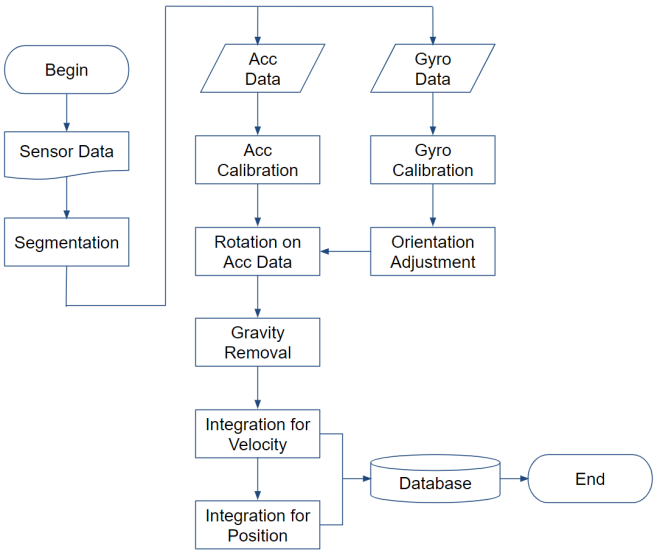

Fig. 3: The flowchart of our proposed system.

E. Gravity Removal

When we place an IMU sensor on an ideally flat surface, the acceleration data it collects should be (X, Y, Z) = (0, 0, 1) due to the gravity on the Z-axis. However, our IMU sensor may not be placed on a perfectly flat surface in practice such that the gravity contributes to the other axes. Since we need to eliminate the influence of gravity, we propose a method of gravity removal. We collect acceleration data in a steady state for one second and subtract the mean of these 400 acceleration data from a_i^{rot} to obtain acceleration data with removing gravity a_i^{rem}.

$$a_i^{rem} = a_i^{rot} - \frac{1}{400} \sum_{j=1}^{400} a_i^{steady}(j) \tag{27}$$

After completing this process, the acceleration data a_i^{rem} can be doubly integrated to obtain correct position information.

F. Overall Flow

The flowchart of the proposed system is shown in Fig. 3. First, our IMU sensor is connected to the computer. Once receiving the data from the IMU sensor, we divide the boxer's punchings into moving segments. Then, these moving segment data are used to construct the trajectories. We calibrate the acceleration and gyroscope data with different calibration methods. Next, we rotate the acceleration data into the same coordinate system via quaternion operations and remove the influence of gravity. Last, we integrate the acceleration data once with respect to time to get the velocity, and integrate the velocity again for having the position information of the trajectory. Furthermore, we upload the results into a database for any further applications.

IV. Experimental Results

In this section, we conduct three experiments and present the results. The first experiment is to show the accuracy of data segmentation. The second experiment is to demonstrate the trajectories of three types of punches, including straight punch, hook, and uppercut. The last experiment is to show the effectiveness of calibration. The results are summarized in TABLE I, TABLE II, and TABLE III, respectively.

A. Data Segmentation

For the first experiment, we invited 5 participants to throw any types of punches consecutively within a certain period of time in 10 punching trials. Then, we count the number of punches identified. We used a camera to record the whole punching process such that the ground truth can be obtained by examining the video. We use mean absolute percentage error ($MAPE$) as a metric to evaluate the accuracy of data segmentation. The $MAPE$ is calculated as EQ(28) where $c^{(i)}$, $c^{(g)}$, and n are the number of identified punches, ground truth, and the number of participants, respectively. In TABLE I, it records the punch counts in all 10 trials with the form of ($c^{(i)}$/$c^{(g)}$) from Column 2 to Column 11. The last column shows the $MAPE$ in data segmentation, which is 3.6%. According to the experimental result, our approach can effectively segment a sequence of punchings into punches.

$$MAPE = \frac{1}{n}\sum_{j=1}^{n}\left|\frac{c_j^{(g)} - c_j^{(i)}}{c_j^{(g)}}\right| \times 100\% \tag{28}$$

B. Trajectory

For the accuracy of trajectories, we tie the IMU sensor and motion marker on the boxer's wrist. The data collected from the IMU sensor will be used to calculate the punching trajectory by the proposed algorithm, and the motion marker will be used with VICON Motion Systems to obtain measurements as ground truth. We calculate the root mean square error ($RMSE$) of the position of the punches. The $RMSE$ is calculated as EQ(29) where n, $p^{(s)}$, and $p^{(v)}$ are the number of data point in one punch, the trajectory obtained by the sensor in our approach, and by VICON Motion Systems, respectively. According to TABLE II, the $RMSE$ of the straight punch, hook, and uppercut are shown in Column 2, Column 3, and Column 4, respectively. The last row record the average $RMSE$ in straight punch, hook, and uppercut, which is 0.041m, 0.078m, and 0.117m, respectively.

$$RMSE = \sqrt{\frac{\sum_{i=1}^{n}(p_i^{(s)} - p_i^{(v)})^2}{n}} \tag{29}$$

Figs. 4(a), 4(b), 4(c) show 3D trajectories of straight punch, hook, and uppercut, respectively. On the right-hand side of the figures, two trajectories are plotted. The green solid line represents the trajectory obtained by our approach while the blue line is the ground truth obtained by the VICON Motion Systems. Additionally, the red circle indicates the starting point of the punches. To have a better illustration of the trajectory results, Figs. 4(a), 4(b) can be viewed from a bird's-eye perspective, and Fig. 4(c) can be viewed from a side angle. Furthermore, we provide a picture of a person on the left-hand side of the figures demonstrating the corresponding punch.

C. Effectiveness of Calibration

As we mentioned in Section III.C, we integrated uncalibrated and calibrated angular velocity once to check which rotation angles is closer to 180°. From the experimental results, both rotation angles are very close to 180°. Although there is not a significant difference between two rotation angles, there are improvements in $RMSE$ when calculating trajectories with the calibrated gyroscope data. In TABLE III, the $RMSE$ without gyroscope calibration and with gyroscope calibration are recorded from Column 2 to Column 4, and Column 8 to Column 10, respectively. According to the experimental results, the average $RMSE$ is lower when gyroscope calibration is applied compared to that not applied, which shows the effectiveness of gyroscope calibration.

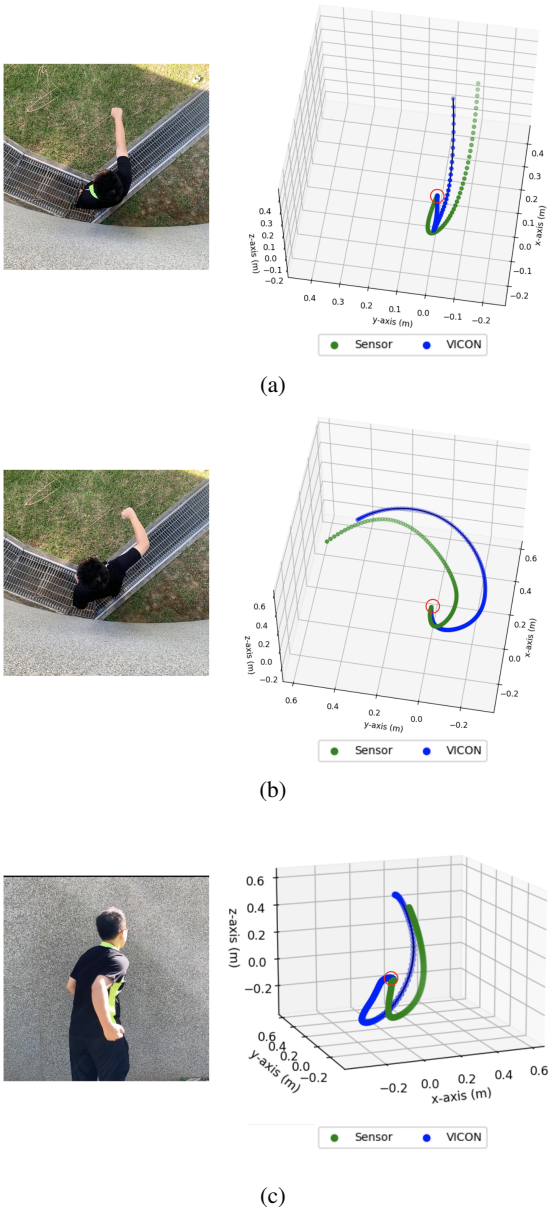

Fig. 4: 3D trajectory of different punches. (a) Straight Punch. (b) Hook. (c) Uppercut.

For the effectiveness of calibration in accelerometer, we integrated uncalibrated and calibrated accelerometer data twice to compare the distance of 0.5m. From the experimental results, using uncalibrated accelerometer data yielded 0.37m, while using calibrated accelerometer data yielded 0.48m. In comparison, integrating calibrated accelerometer data twice obtain a result closer to 0.5m, which shows the importance of this calibration. Moreover, TABLE III shows the $RMSE$ without accelerometer calibration and with accelerometer calibration from Column 5 to Column 7, and Column 8 to Column 10, respectively. According to the experimental results, the average $RMSE$ is lower when accelerometer calibration is applied, which shows the effectiveness of accelerometer calibration as well.

V. Conclusion

In this paper, we present an IMU-based system to construct the trajectory of boxer's punches. This system can be used for sport performance monitoring. According to the experimental

TABLE I: The MAPE in data segmentation.

Trial / *Subject*	1	2	3	4	5	6	7	8	9	10	Absolute Error Rate of Punch Count
A	4/4	4/5	5/5	5/6	6/6	14/15	13/13	13/11	14/15	15/15	0.02
B	3/3	2/2	4/3	3/3	2/2	11/11	10/9	11/11	10/10	12/12	0.03
C	4/5	11/11	5/5	6/6	12/13	6/7	6/6	11/9	8/9	4/6	0.05
D	4/6	8/8	9/9	5/6	7/7	7/9	11/13	23/20	5/5	7/8	0.05
E	5/6	7/8	4/6	6/6	11/9	11/12	7/7	8/9	17/16	17/17	0.03
MAPE	—										3.6%

TABLE II: The RMSE of trajectory in straight punch, hook, and uppercut.

Subject	Straight Punch	Hook	Uppercut
A	0.030	0.067	0.097
B	0.039	0.095	0.117
C	0.023	0.076	0.089
D	0.064	0.082	0.134
E	0.053	0.071	0.148
Average	0.041	0.078	0.117

TABLE III: The RMSE of trajectory in straight punch, hook, and uppercut under different calibration conditions.

Subject	Without Gyro Calibration			Without Acc Calibration			With Gyro & Acc Calibration		
	Straight Punch	Hook	Uppercut	Striaght Punch	Hook	Uppercut	Staight Punch	Hook	Uppercut
A	0.037	0.083	0.124	0.048	0.112	0.151	0.030	0.067	0.097
B	0.044	0.108	0.142	0.053	0.139	0.196	0.039	0.095	0.117
C	0.031	0.085	0.103	0.050	0.119	0.176	0.023	0.076	0.089
D	0.051	0.099	0.156	0.088	0.146	0.203	0.064	0.082	0.134
E	0.055	0.087	0.167	0.091	0.154	0.258	0.053	0.071	0.148
Average	0.043	0.092	0.138	0.066	0.134	0.196	0.041	0.078	0.117

results, our system can construct reliable trajectories compared with a professional motion camera system.

REFERENCES

[1] A. Ahmadi, F. Destelle, D. Monaghan, N. E. O'Connor, C. Richter and K. Moran, "A Framework For Comprehensive Analysis of a Swing in Sports Using Low-cost Inertial Sensors," in *Proc. IEEE SENSORS*, pp. 2211-2214, 2014.

[2] C.-J. Chen, Y.-T. Lin, C.-C. Lin, Y.-C. Chen, Y.-J. Lee and C.-Y. Wang, "Rehabilitation System for Limbs using IMUs," in *Proc. International Symposium on Quality Electronic Design*, pp. 285-291, 2020.

[3] C. Chen, C. X. Lu, J. Wahlström, A. Markham and N. Trigoni, "Deep Neural Network Based Inertial Odometry Using Low-Cost Inertial Measurement Units," *IEEE Transactions on Mobile Computing*, vol. 20, no. 4, pp. 1351-1364, 2021.

[4] Y.-P. Chang, T.-C. Wang, Y.-J. Lee, C.-C. Lin, Y.-C. Chen and C.-Y. Wang, "A Smart Single-Sensor Device for Instantaneously Monitoring Lower Limb Exercises," in *Proc. International System-on-Chip Conference*, pp. 197-202, 2019.

[5] Y.-L. Chen, I.-J. Yang, L.-C. Fu, J.-S. Lai, H.-W. Liang and L. Lu, "IMU-Based Estimation of Lower Limb Motion Trajectory With Graph Convolution Network," *IEEE Sensors Journal*, vol. 21, no. 21, pp. 24549-24557, 2021.

[6] I. Khasanshin, "Application of an Artificial Neural Network to Automate the Measurement of Kinematic Characteristics of Punches in Boxing," *Applied Sciences*, vol. 11, no. 3, pp. 1223, 2021.

[7] Y.-T. Lin, C.-J. Chen, P.-Y. Kuo, S.-H. Lee, C.-C. Lin, Y.-J. Lee, Y.-T. Li, Y.-C.Chen and C.-Y. Wang, "An IMU-aided Fitness System," in *Proc. International System-on-Chip Conference*, pp. 224-229, 2021.

[8] M. Pedley, "High Precision Calibration of a Three-axis Accelerometer," Freescale Semiconductor, Inc., Austin, TX, USA, Application Note AN4399, 2015.

[9] T.-Y. Pan, C.-H. Kuo, H.-T. Liu and M.-C. Hu, "Handwriting Trajectory Reconstruction Using Low-Cost IMU," *IEEE Transactions on Emerging Topics in Computational Intelligence*, vol. 3, no. 3, pp. 261-270, 2019.

[10] T.-Y. Pan, W.-L. Tsai, C.-Y. Chang, C.-W. Yeh and M.-C. Hu, "A Hierarchical Hand Gesture Recognition Framework for Sports Referee Training-Based EMG and Accelerometer Sensors," *IEEE Transactions on Cybernetics*, vol. 52, no. 5, pp. 3172-3183, 2022.

[11] J. Rueterbories, E.G. Spaich, B. Larsen, O.K. Andersen, "Methods For Gait Event Detection and Analysis in Ambulatory Systems," *Medical engineering & physics*, pp. 545-552, 2010.

[12] Tao W, Liu T, Zheng R, Feng H, "Gait Analysis Using Wearable Sensors," *Sensors*, pp. 2255-2283, 2012.

[13] T.-C. Wang, Y.-P. Chang, C.-J. Chen, Y.-J. Lee, C.-C. Lin, Y.-C. Chen and C.-Y. Wang, "IMU-based Smart Knee Pad for Walking Distance and Stride Count Measurement," in *Proc. International Symposium on Quality Electronic Design*, pp. 173-178, 2020.

[14] J. Wu, L. Sun and R. Jafari, "A Wearable System for Recognizing American Sign Language in Real-Time Using IMU and Surface EMG Sensors," *IEEE Journal of Biomedical and Health Informatics*, vol. 20, no. 5, pp. 1281-1290, 2016.

[15] R. Xie and J. Cao, "Accelerometer-Based Hand Gesture Recognition by Neural Network and Similarity Matching," *IEEE Sensors Journal*, vol. 16, no. 11, pp. 4537-4545, 2016.

[16] C. Yu, T.-Y. Huang, and H.-P. Ma, "Motion Analysis of Football Kick Based on an IMU Sensor," *Sensors*, vol. 22, no. 16, pp. 6244-6257, 2022.

[17] Cizmic D, Hoelbling D, Baranyi R, Breiteneder R, Grechenig T. Smart Boxing Glove "RD α": IMU Combined with Force Sensor for Highly Accurate Technique and Target Recognition Using Machine Learning. Applied Sciences. 2023; 13(16):9073.

[18] Khasanshin, Ilshat. 2021. "Application of an Artificial Neural Network to Automate the Measurement of Kinematic Characteristics of Punches in Boxing" Applied Sciences 11, no. 3: 1223.

[19] A. Labintsev, I. Khasanshin, D. Balashov, M. Bocharov and K. Bublikov, "Recognition Punches in Karate Using Acceleration Sensors and Convolution Neural Networks," in IEEE Access, vol. 9, pp. 138106-138119, 2021, doi: 10.1109/ACCESS.2021.3118038.

[20] VICON Motion Systems, https://www.vicon.com/.

[21] Sea Land Technology Inc, https://sealandtech.com.tw/.